Hindawi
Mathematical Problems in Engineering
Volume 2018, Article ID 3121604, 15 pages
https://doi.org/10.1155/2018/3121604

Research Article

Soil-Rock Slope Stability Analysis by Considering the Nonuniformity of Rocks

Shunqing Liu[1], **Xianwen Huang**[1], **Aizhao Zhou**[1], **Jun Hu**[2] and **Wei Wang**[3]

[1]*Department of Civil and Architecture Engineering, Jiangsu University of Science and Technology, Zhenjiang, Jiangsu 212003, China*
[2]*College of Civil Engineering and Architecture, Hainan University, Haikou, Hainan 570228, China*
[3]*School of Civil Engineering, Shaoxing University, Shaoxing, Zhejiang 312000, China*

Correspondence should be addressed to Wei Wang; wangwells@qq.com

Received 28 June 2018; Revised 15 September 2018; Accepted 25 October 2018; Published 8 November 2018

Academic Editor: Payman Jalali

Soil-rock slopes are widely distributed around the world, while the commonly adopted method by simplifying it as a uniform media tends to be excessively conservative. In this study, a slope stability analysis method considering the nonuniform characteristics of rocks was proposed. It was found that the distribution, relative position, and shape of rock have significant effect on slope stability. For the influence of distribution, large rocks at the foot of slope have the most significant effect on slope stability while the effect is insignificant when the rocks are on the slope surface. In terms of the relative position of rocks, four plastic expansion modes of bypass, diversion, inclusion, and penetration were put forward through the analysis on the expansion mode of the plastic zone. Moreover, rock shape also has influence on slope stability.

1. Introduction

Soil-rock slopes are present in most mountainous areas all over the world, especially in the western China region [1, 2]. According to statistics, six of every seven landslide accidents that occurred on the Sichuan-Tibet Highway were associated with soil-rock slopes, along which the earthwork prone to landslides amounted to 300 million m^3. In addition, according to Liao's statistical data on the 816 historical landslide accidents reported in the Panxi area by the end of 2006, 500 landslide accidents, about 61.3% were associated with soil-rock slopes, indicating that soil-rock slopes account for a large proportion of slope accidents [3]. In July 2010, 29 people were killed and several others missing in the landslide of the soil-rock slopes in Zhaizigou, Shanxi Province. In May 2011, a large landslide occurred in Luojiang Village, Guangxi Province, in which the quantity of earth and rock that was dislocated amounted to 200,000 m^3, and caused economic losses of millions of dollars. In June 2017, 10 people were killed and 73 went missing in the massive landslide that occurred in Maoxian County, Sichuan Province, and the length of the river blockage area caused by the landslide reached 2 km. From these, it can be seen that landslide hazards are great threats to the life and property of humans and so it is necessary to prevent them [4]. Compared to homogeneous soil slope and cement-based material-treated soil slope, the nonhomogeneous soil-rock slope may have long and twisted developing path of plastic area because of the rock existing, which produces bigger safety factor [5–7]. Traditionally, soil-rock slope is often considered as homogeneous like soil slope [8–10]. This method of simplifying the soil-rock slope as a homogeneous soil slope neglects the enhancement of rock distribution on slope stability, and the over-conservative assumption is likely to cause wastage of resources. Therefore, it is imperative to analyze the stability and failure characteristics of soil-rock slopes based on the rock distribution, adopting an economical and reasonable support scheme for soil-rock slopes. Soil-rock slopes are mainly composed of soil-rock mixture, which is an extremely uneven multi-phase rock mass material [11, 12].

The mechanical properties of the soil-rock mixture from different aspects, such as stone content, rock shape, rock distribution, position, and bonding strength of the soil-rock interface, have been studied by many scholars. Sonmez

[13] adopted a serious triaxial tests without lateral constraints, proving that the rock content and size can have great influence on the compressing strength, and putting forward prediction formula whose versatility about all kinds of mixtures is not confirmed till now. Gong Jian [14] adopted discrete element method to make research on the effect of rock content to shear strength of soil-rock mixtures including cohesion and friction angel, and then based on the theory of Taylor, explaining the greater shear strength of mixtures which is owing to the contribution of interlocking of rocks. Zhang [15] according to the rock characteristic which is extracted from the slope photos in view, setting many models about soil-rock mixtures with many different sizes. Through analysis, it had be proved that the shape of modulus have influence on the strength characteristic of mixtures and put forward that the arrangement and distribution of rocks are the main factors, which is good agreement with the conclusion of Meng [16]. Fragaszy [17] presented a numerical homogenization study of the elastic property of a soil-rock mixture using random mesostructure generation. Through analysis, it can be found that the connection and broken of bigger rocks are the two main controlling factors to the strength of mixtures. For better evaluating the mechanical characteristic of soil-rock mixtures in engineering, Zhang [18] made a serious in situ test of the soil-rock mixtures in Nuozhadu embankment dam. The results showed that the elastic modulus and friction angel of soil-rock mixtures is bigger than uniform soils obviously, but the cohesion is smaller than soils. There have been extensive studies and research advances regarding the mechanical properties of soil-rock mixtures, while research progress on soil-rock slopes is relatively slow.

Ohene [19] and Hencher [20] put forward a series of stability analysis methods and the concept of slope treatment on slide rock and colluvial landslides based on a large number of site surveys. Liu [21] adopted two different media to simulate the soil and rock and set up corresponding soil-rock slope in random and then studied the the destructive mode and safety factor of slopes. Through analysis, it can be found that the destructive mode of slopes is complicated but the safety factor of it is predictable. Wu [22], based on the elastic-plastic modulus of soil, put forward an calculation modulus of soil-rock slopes considering the interaction of soil and rocks and obtained the conclusion that the soil-rock interaction has a great influence on the landslide shape in terms of rock size and slope angle and the deformation characteristics of landslide at the slope toe is slightly different with that at the slope top. Xu [23] designed a program about polygonal creation which is used to set up soil-rock slopes, and discrete element method is used to simulate the destructive progress and shear band of soil-rock mixtures which were expended in the safe analysis of soil-rock slope finally. Through analysis, it can be proved that the rock shape have a great influence on the shear band developing of soil-rock slope. Maria [5] based on the different rock content and set up a serious 2D slope modulus randomly and then adopted finite element and limit equilibrium methods to study the stability of slope and plastic zone expansion mode. So the conclusion can be achieved that the distribution of rocks can have influence on the stability and safety factor of slopes, but the size of influence is not been discussed and the mechanism of how the rocks affect the plastic zone expansion mode detailed. So it is necessary to study the stability of slopes under the effect of rocks in the slope and put forward a reliable way to analyze the safety of soil-rock slope.

Based on the above reasons, a method for the stability analysis of soil-rock slopes based on the rock distribution and positions is proposed in this paper. The main ideas are as follows. (1) extraction of the original rock position and grading parameters, (2) generating the corresponding random rock contour lines according to rock parameters, (3) using the finite difference finite element method to establish and analyze the corresponding model, and (4) evaluating the stability of the soil-rock slopes through a large number of stability analysis results combined with engineering experience.

2. Random Model Establishment

2.1. Acquisition of Rock Properties. There are two common methods for obtaining the structural parameters of the slope model, namely, CT scanning of unimpaired slopes, obtaining the distribution, location, and rock shape in the slope by nondestructive testing. Li [24] reconstructed the original model by CT scanning, and then compared the results of the numerical simulation with experimental results, obtaining good consistency between the results and thereby establishing the reliability of the model reconstruction for the original slope simulation. Although this method could accurately reflect the distribution characteristics of rock in the original slope, it is the complex preliminary work required limited its applicability for actual projects. Another method is to randomly analyze the slope parameters, such as rock gradation, stone content and distribution location, in the original slope through analogy, reasoning, small-scale in-situ tests, and other methods [25, 26]. Slope safety was evaluated on the basis of a large number of numerical analysis results combined with engineering experience. This method has the advantages of convenient operation and accurately calculated results compared with CT scanning and other in situ tests. Therefore, in this paper, the stability of soil-rock slopes was mainly analyzed by the second method, and this method for obtaining the rock outline would be described in detail as follows.

(1) The method of analogy analysis was adopted to accurately reflect the structural characteristics of the regenerated soil-rock slopes, and a photograph of the slope section adjacent to which a landslide had occurred was captured. Then, using the software Adobe Photoshop, rocks and soil were identified on the basis of the RGB color difference between them, and the corresponding binary image was generated as shown in Figure 1.

(2) Considering the large number of rocks, the artificial identification of the rock area, stone content, distortion coefficient, and other characteristics was a complex process, and the feasibility was not high. Therefore, the relevant computer code was written, and a program was used to identify them. First, the preprocessed image was meshed

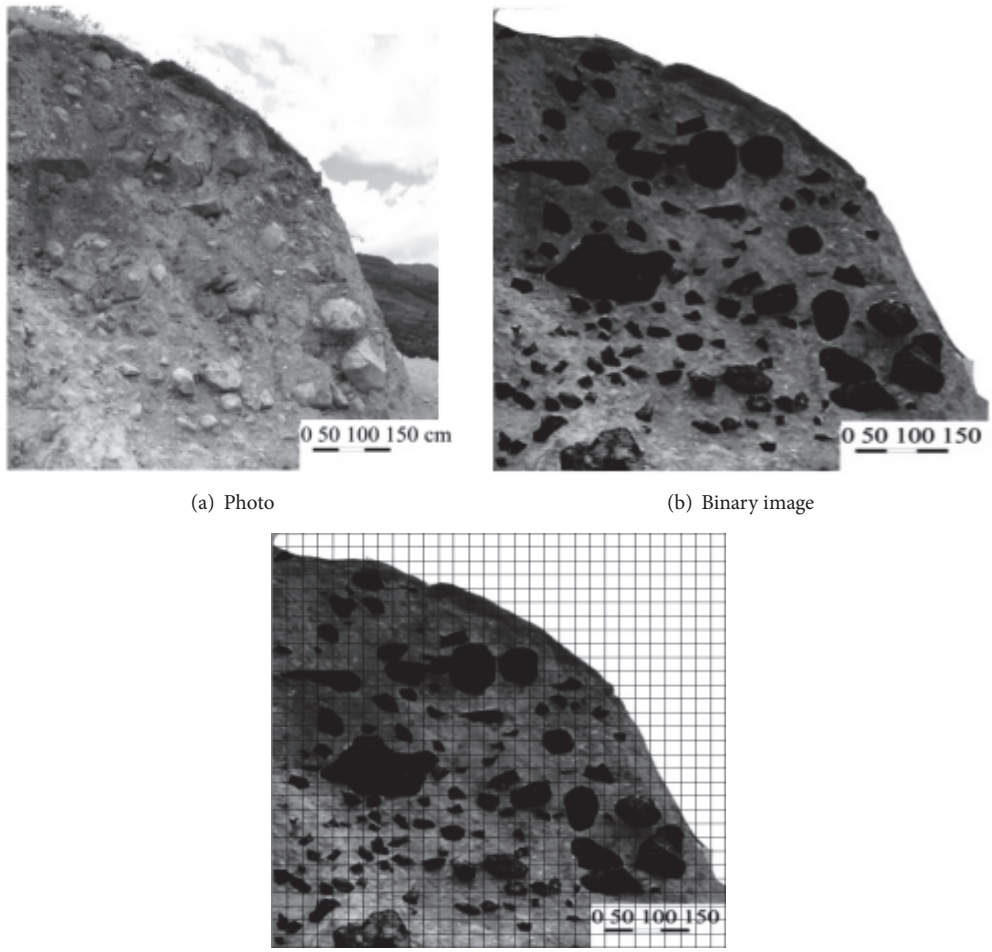

(a) Photo

(b) Binary image

(c) Grid partition

Figure 1: Imaging processing.

finely and evenly, and ten thousand grid points with definite coordinate positions were generated and written into the array. Then, the RGB colors at each grid point were identified, and they were written in the corresponding grid array, as shown in Figure 1(c).

(3) This step involved the identification of the entire rock. The expansion calculation was conducted on the defined rock unit according to the order of the first X axis and the rear Y axis. As shown in the Figure 2, unit a with the position coordinates of (X_a, Y_a) was judged as rock, and a number designating it as stone or rock was assigned to the unit according to the sequence. The coordinates of the eight units in the periphery of a were $(X_a \pm 1, Y_a \pm 1)$, $(X_a, Y_a \pm 1)$, and $(X_a \pm 1, Y_a)$, respectively, and if they contained rock units, the whole unit was assigned the same rock number as unit a. All the rocks were thus merged and identified, and assigned individual codes as the process proceeded, and the result of this process is shown in Figure 2(a).

(4) The final process was the calculation of the rock denaturation. Assuming that an entire rock is assigned the same rock number, the maximum diameter $d_{\max}$, minimum diameter $d_{\min}$, and distortion coefficient $\delta = d_{\max}/d_{\min}$ of the corresponding rock were calculated according to the formula $\sqrt{(X_i - X_j)^2 + (Y_i - Y_j)^2}$. Finally, the corresponding rock area rate and distortion coefficient were obtained through the comprehensive analysis of all the grids, and the result of the calculation was shown in Figure 2(b). In this figure, the minimum diameter is the distance from the center of area with maximum diameter to the outside edge of nearest rock.

2.2. Random Rock Contour Generation. After the image processing of the soil-rock slopes, the corresponding rock area rate and distortion coefficient of the gradation were obtained, and then the rocks in the corresponding gradation section were generated. The method used in this study was to generate a random circle corresponding with the gradation, using it to control the position and maximum diameter of the aggregates, and the corresponding alphabetic strings were x_o, y_o, d. The maximum diameter angle was set as $\theta(i_{\max}) = 2\pi\text{rand}$ (where rand indicates a random value between 0 and

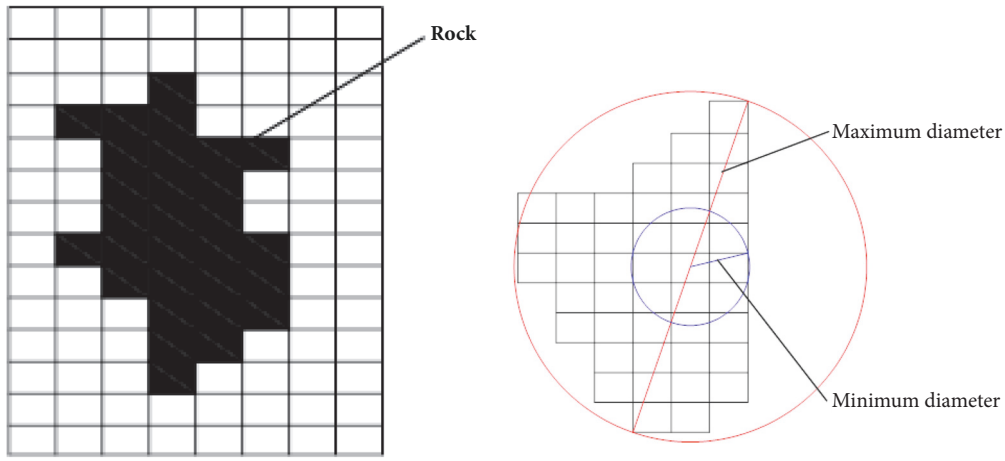

(a) Rock integrity (b) Distortion coefficient of rock

Figure 2: Calculation effect.

1), and the corresponding extreme point coordinates were as follows:

$$\left(x_o \pm 0.5d\cos\left(\theta_{\max}\right), y_o \pm 0.5d\sin\left(\theta_{\max}\right)\right) \quad (1)$$

$$\left(x_o \pm 0.5\delta\cos\left(\theta_{\min}\right), y_o \pm 0.5\delta\sin\left(\theta_{\min}\right)\right) \quad (2)$$

where δ is the random side length under the influence of the distortion coefficient and the calculation formula is $\delta = (1 + k(2\text{rand} - 1))\mu d$, where k represents the variation threshold value of the distortion coefficient (between 0 and 0.1) and μ represents the distortion coefficient (between 0 and 0.9).

After the control points were generated, the assistant random boundary points of the rocks were generated, and the random functions of diameters and angles were $d_{\text{rand}} = \delta + (d - \delta)\text{rand}$ and $\theta_{\text{rand}} = 2\pi\text{rand}$, respectively. Thus, the boundary point coordinates of different rocks could be calculated according to the coordinates of the center point of the circle, and the set maximum polygon edge number (n-4) was taken as the control standard of the calculation number. As the boundary points were of randomly selected angles, all the boundary points of a single rock need to be sorted counterclockwise.

The rock area with rationalization of the boundary point was calculated using the triangle summation method. For any polygon A1, A2,..., with the circle (x_o, y_o) as the triangle vertex and l_{ab} as the bottom edge, the formula for calculating the area of any triangle is

$$S_i = \frac{1}{2}\begin{vmatrix} x_o & y_o & 1 \\ x_n & y_n & 1 \\ x_{n+1} & y_{n+1} & 1 \end{vmatrix} \quad (3)$$

The area of a single rock is obtained as $S = \sum S_i$.

2.3. Release of Rocks. To judge the possibility of invasion between polygonal rocks, the vector area method, and the included angle sum test method were proposed by previous works [27, 28], while DE and Taerwe [29] used the space partition-filling method. Although all the three methods can be used to determine whether or not rocks invade, the calculations are all rather complicated. In this study, the area determination method was adopted to directly judge whether or not the rocks invade by optimizing the release, hence simplifying the complex invasion judgment process. The probability of the random circle inside of the rock was avoided on the basis of the descending order of release gradation, greatly improving the rock release efficiency.

The release process of the rocks was as follows (shown in Figure 3): ① inputting initial parameters, including slope profile function, rock gradation parameters, stone content, and distortion parameters; ② generating the random circle based on the prescribed gradation; ③ determining whether there were rocks invading into the random circle; ④ generating polygonal rocks according to the distortion coefficient, and making node data rationalizations of a single rock; ⑤ drawing the corresponding rock outline map and then repeating steps ②③④ and ⑤ until the system generates an outline map meeting the requirements of the stone content, gradation curve, and distortion coefficient.

2.4. Finite Element Modeling

2.4.1. Finite Difference Strength Reduction Theory. The basis for calculating the slope safety factor in the strength reduction method [30] was that the shear strength parameters of soil were regularly reduced, as shown below:

$$c' = \frac{c}{F_s}$$
$$\varphi' = \arctan\left(\frac{\varphi}{F_s}\right) \quad (4)$$

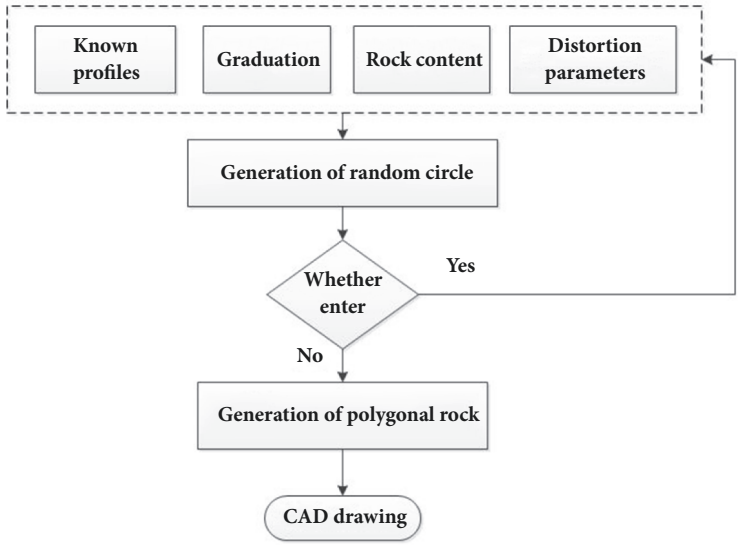

Figure 3: Flow chart of rock generation.

Table 1: Calculation model parameters of soil-rocks slopes.

Constituent	Density (kN/m^3)	Modulus of elasticity (kPa)	Poisson's ratio	Cohesion (kPa)	Internal friction angle (°)
Soil	1.80	50.0	0.35	30	24
Rocks	2.41	2e4	0.2	900	42

When the slope happened to be in the critical damage state, the reduction factor was the safety factor of the slope and the critical failure criterion mainly included

① whether the calculations made by the nonlinear program were convergent

② whether the plastic zone was in state of transfixion and formed a complete plastic zone

③ whether the displacement had a mutation.

In the MIDAS GTS software, the main basis for judging slope instability was whether the nonlinear calculation on energy, displacement, and internal force was convergent. It had the advantages that there was no need to presume the location and geometry of the sliding surface in advance, the influence of the soil deformation on slope stability could be taken into account, the sliding zone could be calculated more accurately, and the safety coefficient could be calculated directly.

2.4.2. Finite Element Model. The randomly generated rock model of the soil-rock slope was imported into the finite element software, and the model was discretized using a triangular mesh, with the maximum unit size being 0.5 times the minimum rock size. The total number of mesh elements was 32550. Horizontal constraints were set on the left and right boundaries of the model, and horizontal and vertical constraints were set at the bottom boundary; in addition, the vertical load due to the self-weight was added to the soil. The physical parameters of rock and soil were shown in Table 1.

2.4.3. Homogeneous Slope Calculation Results. In order to establish the influence relationship of rock locations on the original plastic zone of the slope, the corresponding model of the homogeneous soil slope was established and the sliding zone location was extracted.

As can be seen from Figure 4, the plastic zone started from the foot of the slope and extended to the top of slope. Finally, a perforative sliding zone was formed, and a wedge-shaped slider with a width of 8.34 m was generated in the slope.

Random rock generation software was used to simulate the soil-rock slopes and the strength reduction method was adopted to calculate the slope stability.

It can be seen from Figure 5 that the rock distribution affected the smoothness of the plastic zone. Rocks with high strength blocked the normal development path of the plastic zone, with the slope stability factor increasing to 1.180.

3. Influence of Larger Rock Position on Slope Stability

3.1. Model Feature Description. Four distribution models were established in this paper depending on the relative positions of the rocks and the plastic zone of the homogeneous soil slope. The heights of the areas II, III, and IV were taken based on the trisection of the sliding zone length, and the width of the top of the wedge-shaped slide was considered for the calculations. The area I was the undivided area of the slide, as shown in Figure 6.

An examination of the influence of the rock distribution locations on slope stability indicated that the slope stability

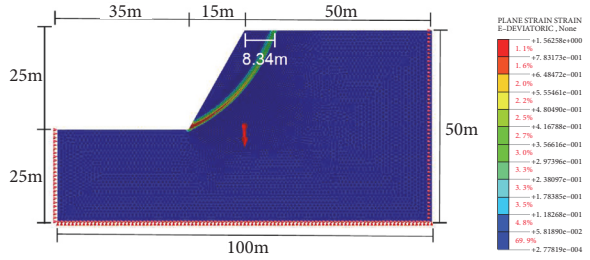

Figure 4: Calculation results of plastic zone in homogeneous soil slope (FOS: 1.01).

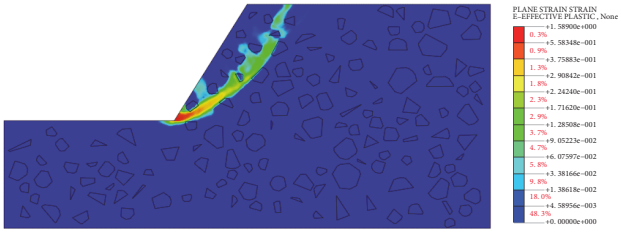

Figure 5: Calculation results of soil-rocks slopes (FOS: 1.18).

could be greatly influenced when the rock diameter was 0.3 times or more the area width by calculating rock models with different sizes. Therefore, the positions of the larger rocks in the slope were given more attention, and the control range of random rock sizes used in calculation was 0.3~0.5 times the width of the entire slope. The four distribution models are shown in Figure 7 were established by adjusting only the positions of the larger rocks, while the stone content and particle shapes were maintained the same.

3.2. Analysis of Calculation Results. As can be seen from Figure 8, the existence of larger rocks caused the originally smooth plastic zone to develop by flocculation, bifurcation and burr, and the plastic zone expansion exhibited an obvious "bypass" effect. The different distribution positions of larger rocks in the slope had different effects on the expansion mode and stability of the plastic zone.

As shown in Figure 8(a), when the larger rocks distributed in area I, the slope stability coefficient increased from 1.01 for the homogeneous soil slope to 1.188. It was assumed that the sliding portion of the slope was a massive block, and the larger rocks were located in the position indicated by area I, that is, the surface of the slope. The larger mass of the rocks made the barycenter of the sliding body deviate to the slope surface. Under the premise that the sliding zone was fixed, the angle of gravity direction of the barycenter of the sliding body and tangential angle of the sliding zone increased. The stress σ_x in the soil in the sliding zone along its normal direction increased, while the stress σ_y in the tangential direction and the shear stress τ decreased, which finally led to the decrease of the sliding force generated by the sliding body. Thus, the slope exhibited a greater safety factor. On the other hand, the smaller rocks in some slopes caused the development

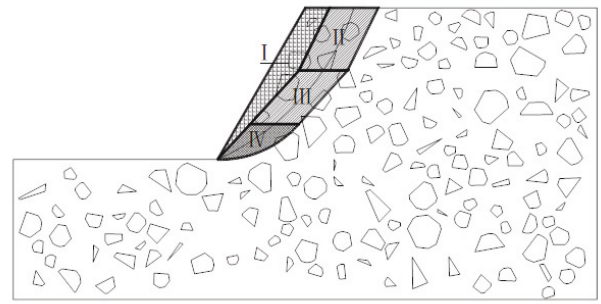

Figure 6: Location division of rocks.

route of the plastic zone in the slope to zigzag, increasing the development length of the plastic zone and improving the slope stability.

The larger rocks were stacked at the upper part of the plastic zone (area II), forming a plastic development area as shown in Figure 8(b). The plasticity development route of the slope was more complicated compared to the original homogeneous soil slope. The distribution pattern of the large rocks directly hindered the development route of the plastic zone at the top of slope, increasing the slope safety factor from 1.010 for homogenous soil to 1.316. Compared with the barycenter offset of the sliding mass in Figure 8(a), the larger rock distribution in this area directly affected the plasticity development route of the slope, making it impossible to form a penetrating and smooth primary plastic zone.

When the larger rocks were predominantly distributed in area III, the slope safety factor was 1.437, which was larger compared to the rock distribution in area II. The distribution of larger rocks in the middle of the slope plasticity development area hindered the development route of the plastic zone, making the formation of a penetrating and smooth primary plastic zone impossible. When the spacing of rocks was smaller, two front and back plastic zones around whole rocks formed. When rocks were spaced closely together, the phenomenon of "inclusion" can be observed, in which the plastic zone is developed first among the rocks and then continues onward to form the main plastic zone and develop further.

As can be seen from Figure 8(d), when larger rocks were distributed at the foot of the slope, there was a significant effect on the slope stability. And the stability coefficient increased from 1.01 for the homogeneous soil slope to 1.492 for the soil-rock mixture. When rocks with higher strength are distributed at the foot of the slope, the plasticity development route gets deviated from the foot of slope to the top of the rock accumulation. The movement of the plastic zone reduced the effective height of the slope in a relative sense and improved the slope stability.

Through the stability analysis of slopes with four different types of large-rock distributions, it was found that their magnitudes and manner of their influence on the slope stability were different. The obtained relationship with slope stability followed the relation Area IV (accumulation of larger

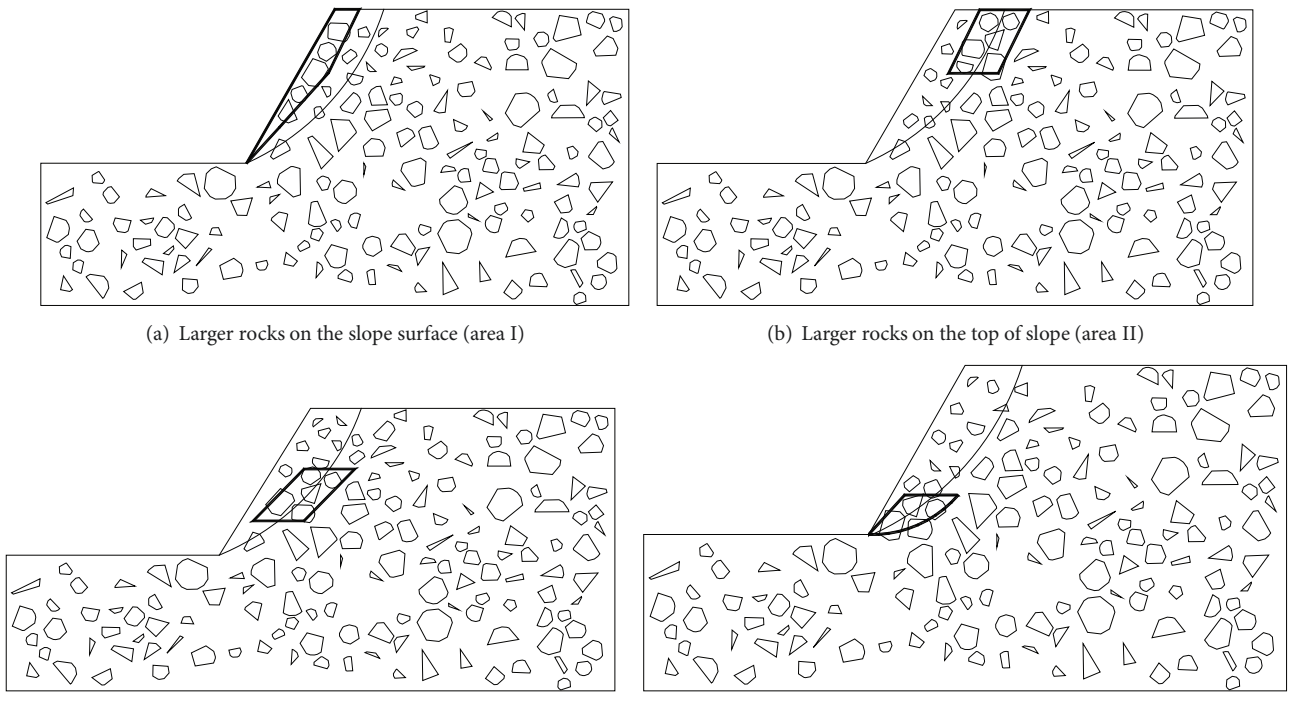

(a) Larger rocks on the slope surface (area I)

(b) Larger rocks on the top of slope (area II)

(c) Larger rocks on the slope surface (area III)

(d) Larger rocks on the top of slope (area IV)

Figure 7: Distribution of larger rocks with four kinds of positions.

rocks at the foot of the slope) > Area III (accumulation at the middle part of the slope) > Area II (accumulation at the top of the slope) > Area I (accumulation at the slope surface).

4. Influence of Relative Spacing of Rocks on Slope Stability

4.1. Model Feature Description. Although the distribution position of larger rocks had a greater impact on the overall slope stability, the impact of the relative position of rocks on slope stability could not be ignored. Even when the larger rocks were distributed within the same area, different relative distances and relative positions caused the plastic zone development to exhibit different patterns, thereby affecting the slope safety factor. According to the relative positions of the rocks, four main modes of plastic zone development were put forward. The condition of crack development in soil-rock mixtures was difficult to measure directly with existing technologies. Therefore, the authors took advantage of the characteristic that crack pairs would form along weak areas when the soil-rock mixture is air-dried. Using air-drying to disturb the soil-rock mixture, the method of replacing the sliding zone of the soil-rock mixture by an air shrinkage crack was used to represent the plasticity extension path in the soil-rock mixture, and Figure 9 shows the four different development modes that were observed using this method.

Mode I: As shown in Figure 9(a1), the larger rocks were distributed in the plastic zone extension path of the original homogeneous soil, causing an offset in the extension path, expanding along the weaker side of the whole rocks, and exhibiting "bypass." As shown in Figure 9(a2), the rocks blocked the primitive crack development of the soil, causing them to develop along the rock edges and changing the path of crack development.

Mode II: As shown in Figure 9(b1), the plastic zone expanded inside the rocks. Due to the greater strength of the rocks, the plastic zone expanded along the larger rocks creating a "tree root" pattern. As shown in Figure 9(b2), the original, single plasticity extension path turned into multiple plasticity extension paths after passing through larger rocks, resulting in the formation of "diversions." It also shows that a single crack divided into two cracks after passing through a block of rocks, which was different from the theoretical trajectory.

Mode III: As shown in Figure 9(c1), a single plasticity expansion path continued to develop in the same manner after entering the larger rock area. The "inclusion" phenomenon of the plastic zone appeared in the rock group; that is, the hitherto separate plastic zones merged into a single main plastic zone and continued to develop after passing around rocks. As shown in Figure 9(c2), obvious cracks appeared around the rocks and the presence of the rocks did not affect the crack development path.

Mode IV: As shown in Figure 9(d1), the plastic zone developed just along the cracks between the rocks, resulting in a "penetration" phenomenon relative to the rock group. As shown in Figure 9(d2), cracks in the soil-rock mixture developed in the interstices between two rocks, giving rise to "penetration."

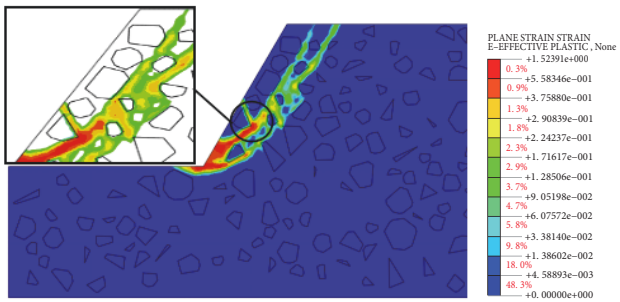

(a) Larger rocks on the slope surface (area I) (FOS=1.188)

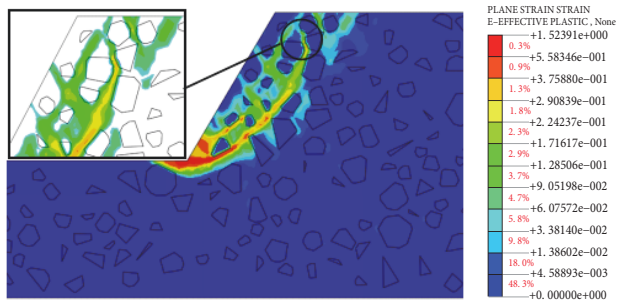

(b) Larger rocks on the top of slope (area II) (FOS=1.316)

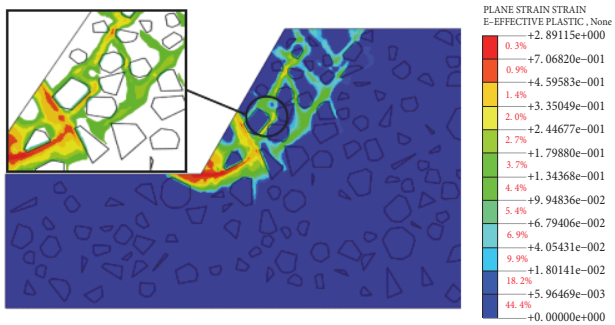

(c) Larger rocks on the slope surface (area III) (FOS=1.437)

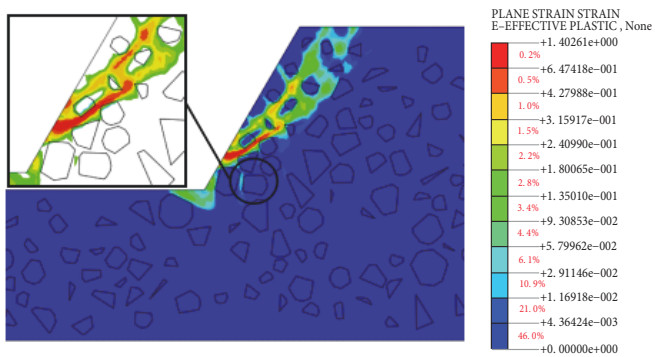

(d) Larger rocks on the top of slope (area IV) (FOS=1.492)

Figure 8: Slope stability calculation results.

4.2. Results of the Analysis

4.2.1. Analysis of Plastic Zone Expansion Mode. By adjusting the relative position of the larger rocks, it was found that the relative position of the rocks had little effect on the plastic zone development path of the slope and the effect on the slope safety factor was smaller when the larger rocks were stacked in area I. Therefore, the slope stability corresponding to larger rocks in the area II, III, and IV alone was analyzed, as shown in Table 2. It can be seen from the table that the slope safety factor manifested certain discreteness under conditions of same rock distribution positions and different relative positions and intervals of rocks.

Regarding the distribution of larger rocks in area II, the slope safety coefficients under the four modes were 1.341, 1.325, 1.316, and 1.275, respectively. As can be seen from Figure A, the close-packed rocks made the plastic zone expand along the edge of the rock stack toward its top. On the one hand, the existence of rock edges and corners made the plastic zone develop along a zigzag path. On the other hand, the higher strength of the rock increased the antislip force of the slope and improved the slope stability. As can be seen from Figure B, the plastic zone was diverted under the action of larger rocks at the top of the slope, and one of the small plastic zones continued to develop, eventually producing a perforative plastic zone on the slope surface. Figure C reflected the development of the plastic zone when it contained rocks, and the existence of larger rocks did not have a significant impact on the plastic zone development. As can be seen in Figure D, the rock distribution did not

Table 2: The results of soil-rocks slopes.

	Model 1	Model 2	Model 3	Model 4
area II	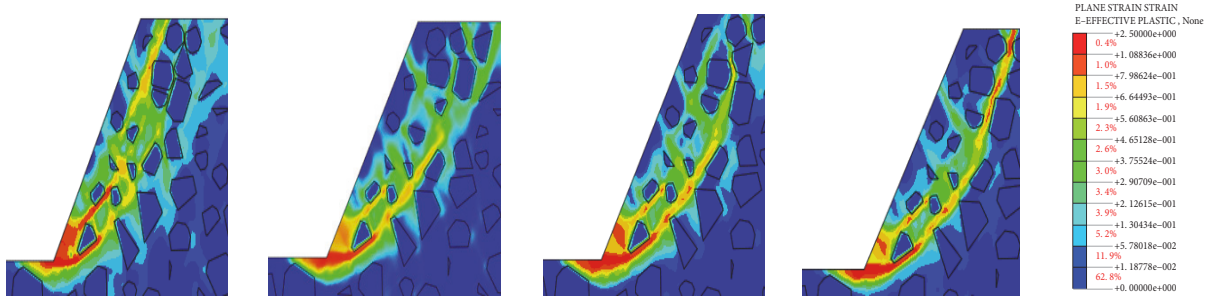			
	Fig. A FOS: 1.341	Fig. B FOS: 1.325	Fig. C FOS: 1.316	Fig. D FOS: 1.275
area III	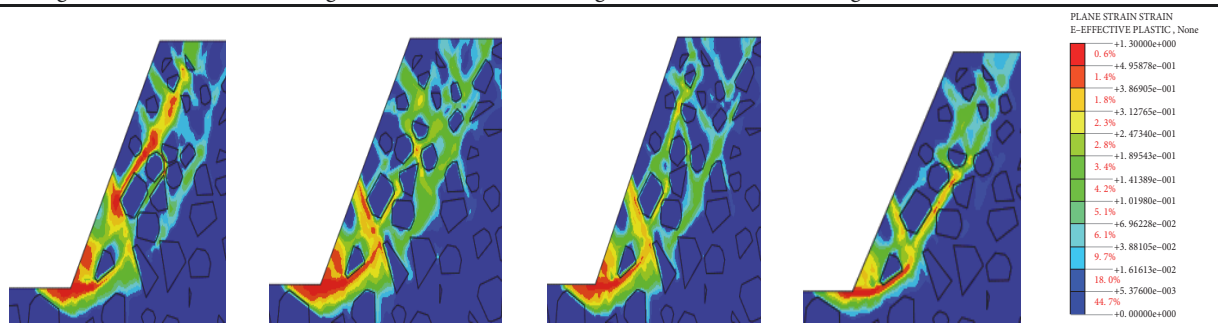			
	Fig. E FOS: 1.424	Fig. F FOS: 1.430	Fig. G FOS: 1.437	Fig. H FOS: 1.322
area IV	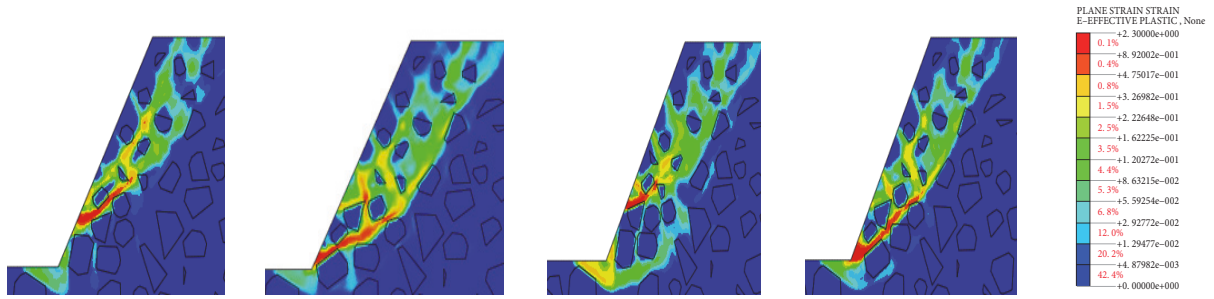			
	Fig. I FOS: 1.519	Fig. J FOS: 1.510	Fig. K FOS: 1.492	Fig. L FOS: 1.407

affect the route of the plastic zone development. Through comprehensive analysis, in this area, the impact of each mode on slope stability follows the order Mode I > Mode II > Mode III > Mode IV.

When the larger rocks were distributed in area III, the slope safety coefficients under the four kinds of modes were 1.424, 1.43, 1.437, and 1.322, respectively. When the spacing between rocks was relatively small, the plastic zone moved along the edge of whole rocks to the slope surface and continued to develop as shown in Figure E. The plastic zone extension lines in Figure F and Figure G are similar. The plastic zone in the area of rock accumulation area in the slope developed along the rock edges and then gradually aggregated into the main plastic zone toward the top of the slope. The rocks in Figure H are distributed around the original plastic zone, and they did not have a significant influence on the path of the plastic zone development. It was determined from the analysis that, in this area, the influence relationship of each mode on slope stability followed the order Mode III > Mode II > Mode I > Mode IV.

The larger rocks distributed at the foot of the slope had the greatest impact on the increase in slope stability, with the corresponding safety factors being 1.519, 1.510, 1.492, and 1.407, respectively. Larger rocks directly obstructed the plastic zone development, making the plastic zone at the foot of the slope extend along the top of the rocks (Figure I). As the relative distance between the rocks increased and the relative position was adjusted, larger rocks at the foot of slope still blocked the onset of the plastic zone (Figure J and K). This indicates that the initial position of the plastic zone would be affected when larger rocks were distributed at the foot of the slope. When rocks were distributed along the plastic zone consisting of homogeneous soil, the influence on the plastic zone development was of a lesser degree and the increase in the slope safety factor was smaller. The results indicate that, in

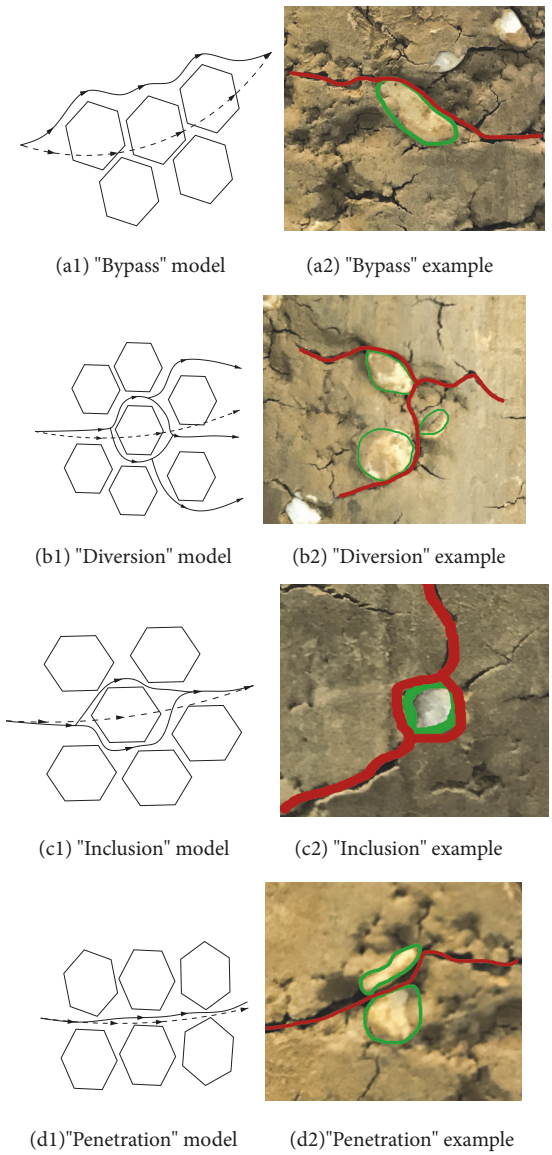

Figure 9: Four plasticity expansion modes.

this area, the impact of each mode on the slope stability was Mode III > Mode II > Mode I > Mode IV.

4.2.2. Slope Stability Analysis. For a given area of accumulation, the relative position of the larger rocks was continuously adjusted to obtain the slope safety factor corresponding to different positions of large-rock accumulation as per the statistical method, as shown in Figure 10.

As can be seen from Figure 10, the slope safety factor varied with the distribution position of larger rocks, showing great discreteness. By comparing the values of the slope safety factor under different large-rock accumulation conditions in each area, it was found that the discreteness of larger rock accumulation in the middle part of slope was the largest. The reason was that the plastic zone in the slope existed mainly in three modes, namely, the "bypass," "inclusion," and "penetration." The three modes influence the expansion

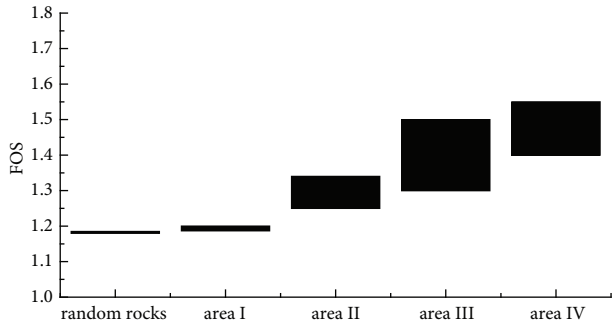

Figure 10: Slope safety factor.

path of the plastic zone to different extents and in different manners, giving rise to greater discreteness. When the larger rocks were accumulated at the foot of the slope, the discrete value of the slope safety factor was 0.15. Here, the plastic zone generally passed through the rock accumulation area in the "bypass" and "penetration" modes, with the former having an impact on the starting position of the plastic zone and the latter increasing the slip resistance of the slope, so that the rock accumulation in this position exhibited a certain degree of discreteness. When the larger rocks were accumulated at the top of the slope, the discrete value of the slope safety factor was 0.11. Here, the plastic zone generally passed through the rock area in the modes of "diversion," "bypass," and "penetration." At the top of the slope where the plastic zone development ended, the slope safety factor exhibited smaller discreteness as long as the plastic zone developed along the weakest path to form a penetrating sliding zone. When the larger rocks were accumulated at the slope surface, the changes in their relative positions did not affect the overall development of the plastic zone; there was a phenomenon of "bypass," and the discrete value of the slope safety factor was only 0.04. When the distribution of the larger rocks was not considered, the discrete value of the slope safety factor was the least, only 0.02.

5. Influence of Stone Shape on Slope Stability

5.1. Description of Model Features. In nature, different geological causes cause the soil-rock mixture to have different shapes [31]. For example, rocks in sedimentary soil-rock mixtures are scoured and transported by water flow for long periods of time, making them relatively smooth. On the other hand, rocks in colluvial soil-rock mixtures exhibit strong angularity, taking on needle-plate like shapes. The difference in rock shapes has a huge impact on the mechanical properties of the soil-rock mixture [32–35]. Nouguier-Lehon [36] based on different rock shapes adopted granular flow software to simulate mechanical properties of soil-rock mixtures and achieved that the rock shape has great influence on the strength of soil-rock mixtures. After that, Xu [37], owing to the use of CT method, adopted the greater shear testing instrument to study the strength characteristic and destructive path of soil-rock mixtures, but they ignore the

rock shape to the strength characteristic and destructive path of soil-rock mixtures.

In this work, based on the study of dry shrinkage cracks in the soil-rock mixture, it was found that there were differences in the crack width and extension for pebbles and gravels, and the development of cracks in pebbles and gravels was analyzed according to the pattern differences, as shown in Figure 11.

Through the comparative analysis of the cracks in pebbles and gravels in the four modes, it was found that cracks usually developed at the ends of the rocks in the case of pebbles, while cracks usually develop along the rock edges and corners in gravels. Combined with the crack numbers and widths shown in Figures 11(e2) and 11(e3), it was found that the cracks were wider for pebbles and there were few microcracks in the periphery, while the cracks associated with the crushed stone were finer, and comparatively more microcracks appeared in the periphery. Therefore, it was believed that pebbles had a certain concentration effect on the crack development of the soil-rock mixture; that is, the cracks were concentrated along the main cracks. Meanwhile, the gravels did not have a concentration effect and the soil cracks were more chaotic. Therefore, it was necessary to analyze the influence of larger rock shapes on slope stability.

In this study, circular and triangular rocks were used to simulate pebbles and gravels respectively. In order to avoid the impact of the rock area ratio on slope stability, the triangle side length was maintained as $l = 2 \bullet 3^{-0.25}\pi^{0.5}r$ (where r is the circle radius) and eight corresponding analytical models were established according to the distribution positions and shapes of the larger rocks.

5.2. Results of the Analysis

5.2.1. Influence of Rock Shape on Slope Stability. As can be seen from the Figure 12, the slope safety factors of round rocks and triangular rocks were 1.268 and 1.273, respectively, when the larger rocks were distributed in area I. From the perspective of the plastic zone development, large round rocks had less influence on the plastic zone development of slope, while larger triangular rocks had a greater impact, which was mainly reflected in the development of the partial plastic zone affected by triangular rock edges and corners.

It could be seen from the Figure 13 that the phenomenon of "bypass" occurred in the plastic zone of the slope under the influence of circular rocks, and the plastic zone continued to develop mainly along rock edges with the slope safety factor increasing to 1.311. When triangular rocks were distributed at the top of the slope, the plastic zone was not single but developed multidirectionally along the rock gap and stress concentrations appeared at the rock edges and corners. The reason was that the circular rock surface was smoother when the plastic zone developed adjacent to the rock surface, which made it easy to guide the plastic zone development along the circular rock edge. However, the triangular rock had sharp edges and corners that did not have a streamlined shape, so the plastic zone developed freely and a more chaotic situation ensued. In addition, the existence of rock edges and corners made stress concentrations easy to occur at rock corners.

When the larger rocks were distributed at the middle part of the slope, the slope safety factors of circular and triangular rocks were 1.421 and 1.516, respectively (Figure 14). The plastic zone mainly developed along rock edges in the slope that consisted of circular rocks. In triangular rocks, a part of the plastic zone developed along the rock edges while there appeared a "flurry" development route due to the action of the rock edges and corners. In addition, stress concentrations developed at the rock edges and corners.

For the larger rocks distributed in area IV (Figure 15), the circular and triangular rocks all impeded the plastic zone development at the foot of the slope, causing the plastic zone at the foot of slope to shift upwards. When the slope consisted of circular rocks, the plastic zone developed along the rock edges, which differed considerably from the plastic zone development path taken when the slope consisted of triangular rocks. The reason was that the relatively smooth edge of the circular rocks had a certain inductive effect on the plastic zone development of the slope.

5.2.2. Discreteness Analysis of Rock Shapes. The distortion values pertaining to the circular and triangular rocks were 1.0 and 0.5, respectively. However, the distortion coefficients of the larger rocks in the actual slope were random, necessitating the statistical analysis of the slope stability under different distortion values, as shown in the Figure 16.

Through the analysis on the slope safety factor with larger rocks under different distortion coefficients in the same area, it was found that the slope safety factor went on increasing as the distortion coefficient decreased. The reason was that the larger the distortion value of rock shape, the closer the rock was to the circle, and the easier it was to induce the plastic zone of the slope to develop along rock edges and form the main plastic zone. However, rocks with relatively small distortion values could easily guide the plastic zone development along their edges and corners, resulting in the phenomenon of "diversion," which made it difficult to produce a main plastic zone. Therefore, the slope safety decreased with the increase of distortion values.

Slope safety factors with larger rocks distributed in different areas were compared, and the order was obtained as Area IV > Area III > Area II > Area I, which was same as the result from the impact analysis and influence of larger rock distribution positions on slope stability obtained in Section 3. In different areas, the differences in rock distortion values made the slope safety factor have a certain degree of dispersion, the magnitude relationship was obtained as Area IV > Area III > Area II > Area I; the difference was mainly reflected in the influence of rock shapes on the plastic zone development path of slope. Circular rocks had smoother outlines compared to polygonal rock, which were more likely to guide the development path of the plastic zone.

6. Conclusion

In this study, Adobe Photoshop software was used to complete the preprocessing of soil-rock slope images, and a custom program was developed to extract the characteristic

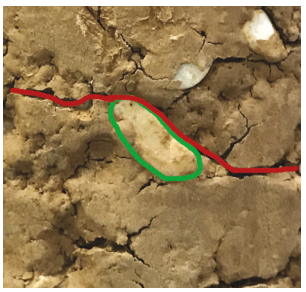

(a2) "Bypass" example of pebbles

(a3) "Bypass" example of gravels

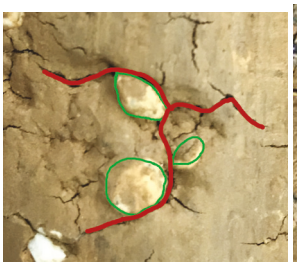

(b2) "Diversion" example of pebbles

(b3) "Diversion" example of gravels

(c2) "Inclusion" example of pebbles

(c3) "Inclusion" example of gravels

(d2) "Penetration" example of pebbles

(d3) "Penetration" example of gravels

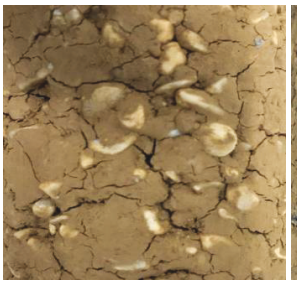

(e2) Cracks of pebbles

(e3) Example of gravels

Figure 11: Cracks of pebbles and gravels.

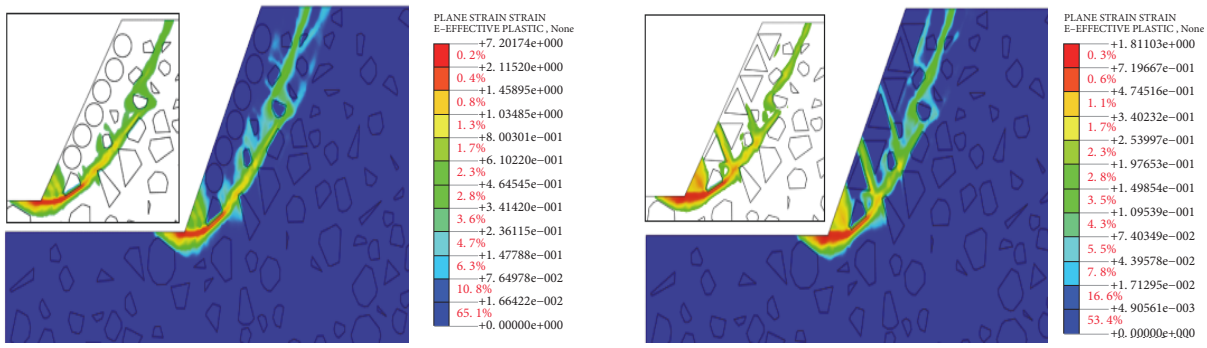

(a) Pebbles FOS=1.268 (b) Gravels FOS=1.273

Figure 12: Plastic zone development cloud chart of slope with accumulation of larger rocks at slope surface.

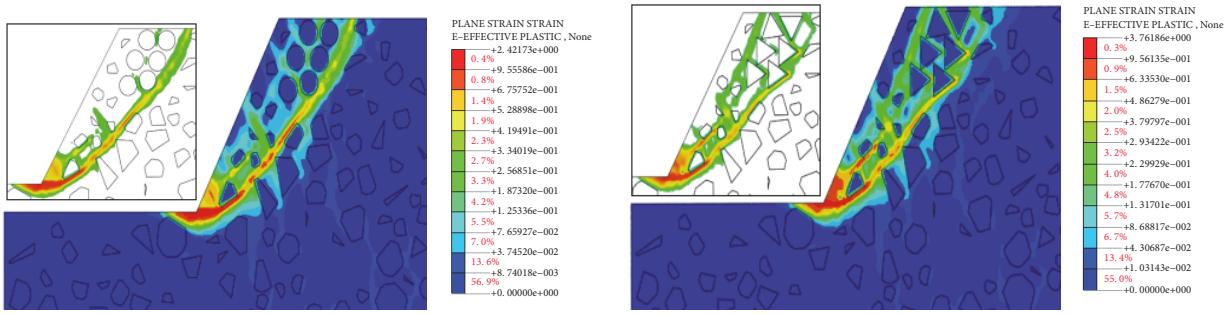

(a) Pebbles FOS=1.311 (b) Gravels FOS=1.334

Figure 13: Plastic zone development cloud chart of slope with accumulation of larger rocks at the top of slope.

parameters of rock in soil-rock slopes by grid partition. Then, the corresponding contour map was drawn in CAD using a VBA code. Finally, the slope stability was analyzed based on the method of finite element strength reduction. Through analysis, the following conclusions were drawn:

(1) Considering the lack of sufficient stability analyses data regarding traditional soil-soil mixture slopes, a stability analysis method for the soil-soil mixture slope based on rock characteristic parameters of the original slope was proposed.

(2) Through the analysis, it was found that the distribution position of larger rocks in the slope had a significant impact on slope stability, and the relationship was ordered as Area IV (accumulation of larger rocks at the foot of slope) > Area III (accumulation at the middle part of slope) > Areas II (accumulation at the top of the slope) > Area I (accumulation at the slope surface).

(3) In the analysis, it was found that the relative positions of the larger rocks had a certain impact on slope stability. The discrete relationship of slope safety factor was obtained as the distribution of larger rocks in Area III > Area IV > Area II > Area I.

(4) Rock shapes also had a certain effect on slope stability. The discrete relationship of slope safety factor was the distribution of larger rocks in Area IV > Area III > Area II > Area I.

(5) Through the analysis, it was found that the distribution of the larger rocks had a great influence on the development and stability of the plastic zone of the slope. When the method in this study is used to calculate the stability of the soil-rock slopes, the actual position of larger rocks in the slope should be surveyed to improve the accuracy of slope stability analysis.

It should be noted that the size effect may play an important role in the calculation result. If the slop is very big or very small, then the distribution and shape effect would be still valid, but it would make difference to the calculated absolute value. To fully capture the performance, some new methods may need to be employed [38]. As a limitation, size effect was not considered in this study, which forms the scope of future investigations.

Data Availability

The data used to support the findings of this study are included within the article.

Conflicts of Interest

The authors declare that they have no conflicts of interest.

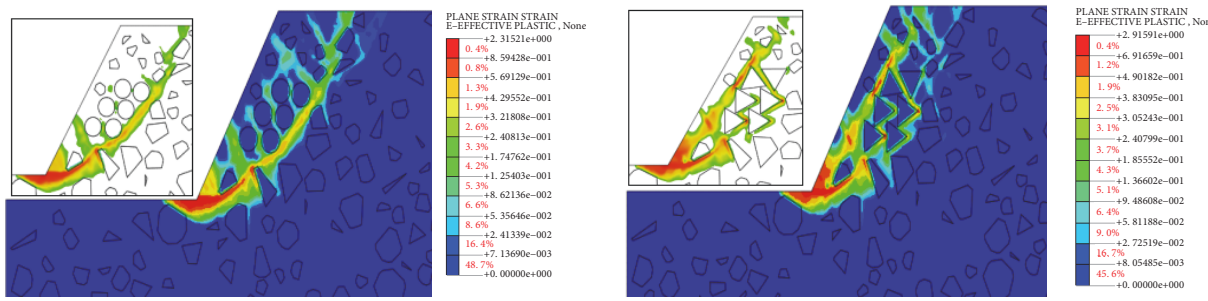

(a) Pebbles FOS=1.421 (b) Gravels FOS=1.516

Figure 14: Plastic zone development cloud chart of slope with accumulation of larger rocks at the middle part of slope.

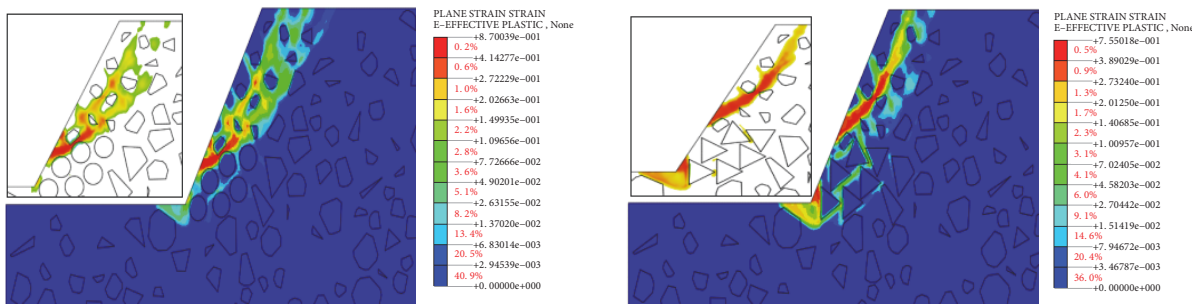

(a) Pebbles FOS=1.441 (b) Gravels FOS=1.572

Figure 15: Plastic zone development cloud chart of slope with accumulation of larger rocks at the foot of slope.

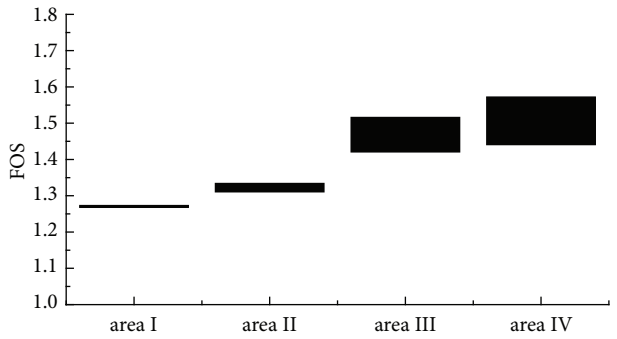

Figure 16: Slope safety factor under different distortion coefficients.

Acknowledgments

This work was supported by the National Natural Science Foundation of China (41772311; 51579199), the Zhejiang Provincial Natural Science Foundation of China (LY17E080016), and the Natural Science Fund for Colleges and Universities of Jiangsu Province (Grant no. 17KJB560003). China Postodoctoral Science Foundation (2018M630722) and Hainan Natural Science Foundation (518MS122, 518QN307) are also acknowledged.

References

[1] G. Vessia, J. Kozubal, and W. Puła, "High dimensional model representation for reliability analyses of complex rock–soil slope stability," *Archives of Civil and Mechanical Engineering*, vol. 17, no. 4, pp. 954–963, 2017.

[2] R. K. Goel and B. Singh, "Engineering rock mass classification," *Petroleum*, pp. 357–365, 2012.

[3] Q. Liao, X. Li, and Z. Hao, "Current status and future trends of studies on rock and soil aggregates," *Engineering Geology*, vol. 14, no. 6, pp. 801–807, 2006.

[4] D. Guo, C. He, C. Xu, and M. Hamada, "Analysis of the relations between slope failure distribution and seismic ground motion during the 2008 Wenchuan earthquake," *Soil Dynamics and Earthquake Engineering*, vol. 72, pp. 99–107, 2015.

[5] M. L. Napoli, M. Barbero, E. Ravera, and C. Scavia, "A stochastic approach to slope stability analysis in bimrocks," *International Journal of Rock Mechanics and Mining Sciences*, vol. 101, pp. 41–49, 2018.

[6] A. Zhou, C. Li, P. Jiang, K. Yao, N. Li, and W. Wang, "Slip Line Theory Based Stability Analysis on the Influence of Deep Excavation on Adjacent Slope," *Mathematical Problems in Engineering*, vol. 2018, Article ID 2041712, 2018.

[7] W. Wang, C. Zhang, N. Li, F. F. Tao, and K. Yao, "Mechanical performance of nanometer magnesia and cement reinforced seashore soft soil by direct shear test," *Marine Georesources & Geotechnology*, 2018.

[8] P. Jiang, L. Qiu, N. Li, W. Wang, A. Zhou, and J. Xiao, "Shearing Performance of Lime-Reinforced Iron Tailing Powder Based on Energy Dissipation," *Advances in Civil Engineering*, vol. 2018, pp. 1–8, 2018.

[9] W. Wang, N. Li, F. Zhang, A. Zhou, and S. Chi, "Experimental and Mathematical Investigations on Unconfined Compressive Behaviour of Costal Soft Soil under Complicated Freezing Processes," *Polish Maritime Research*, vol. 23, no. 4, pp. 112–116, 2016.

[10] Y. Pan, Y. Liu, H. Xiao, F. H. Lee, and K. K. Phoon, "Effect of spatial variability on short- and long-term behaviour of axially-loaded cement-admixed marine clay column," *Computers & Geosciences*, vol. 94, pp. 150–168, 2018.

[11] A. Hamidi, V. Yazdanjou, and N. Salimi, "Shear strength characteristics of sand-gravel mixtures," *International Journal of Geotechnical Engineering*, vol. 3, no. 1, pp. 29–38, 2009.

[12] Y. Wang, X. Li, B. Zheng, and C. F. Ma, "An Experimental Investigation of the Flow–Stress Coupling Characteristics of Soil–Rock Mixture Under Compression," *Transport in Porous Media*, vol. 112, no. 2, pp. 429–450, 2016.

[13] H. Sonmez, M. Ercanoglu, A. Kalender, G. Dagdelenler, and C. Tunusluoglu, "Predicting uniaxial compressive strength and deformation modulus of volcanic bimrock considering engineering dimension," *International Journal of Rock Mechanics and Mining Sciences*, vol. 86, pp. 91–103, 2016.

[14] J. Gong and J. Liu, "Analysis on the mechanical behaviors of soil-rock mixtures using discrete element method," *Procedia Engineering*, vol. 102, pp. 1783–1792, 2015.

[15] S. Zhang, H. Tang, H. Zhan, G. Lei, and H. Cheng, "Investigation of scale effect of numerical unconfined compression strengths of virtual colluvial-deluvial soil-rock mixture," *International Journal of Rock Mechanics and Mining Sciences*, vol. 77, pp. 208–219, 2015.

[16] Q. X. Meng, H. L. Wang, W. Y. Xu, and M. Cai, "A numerical homogenization study of the elastic property of a soil-rock mixture using random mesostructure generation," *Computers & Geosciences*, vol. 98, pp. 48–57, 2018.

[17] R. J. Fragaszy, W. Su, and F. H. Siddiqi, "Effects of oversize particles on the density of clean granular soils," *Geotechnical Testing Journal*, vol. 13, no. 2, pp. 106–114, 1990.

[18] Z.-L. Zhang, W.-J. Xu, W. Xia, and H.-Y. Zhang, "Large-scale in-situ test for mechanical characterization of soil–rock mixture used in an embankment dam," *International Journal of Rock Mechanics and Mining Sciences*, vol. 86, pp. 317–322, 2016.

[19] O. Karikari-Yeboah, "Stability of Slopes characterized by colluviums: investigation, analysis, and stabilization," *Géotechnique*, vol. 10, pp. 47–53, 2000.

[20] S. R. Hencher and D. P. McNicholl, "Engineering in weathered rock," *Quarterly Journal of Engineering Geology and Hydrogeology*, vol. 28, no. 3, pp. 253–266, 1995.

[21] Y. Liu, H. Xiao, K. Yao, J. Hu, and H. Wei, "Rock-soil slope stability analysis by two-phase random media and finite elements," *Geoscience Frontiers*, vol. 9, no. 6, pp. 1649–1655, 2018.

[22] Q. Wu, Y. An, and Q. Liu, "SPH-Based Simulations for Slope Failure Considering Soil-Rock Interaction," *Procedia Engineering*, vol. 102, pp. 1842–1849, 2015.

[23] W.-J. Xu, L.-M. Hu, and W. Gao, "Random generation of the meso-structure of a soil-rock mixture and its application in the study of the mechanical behavior in a landslide dam," *International Journal of Rock Mechanics and Mining Sciences*, vol. 86, pp. 166–178, 2016.

[24] C.-S. Li, D. Zhang, S.-S. Du, and B. Shi, "Computed tomography based numerical simulation for triaxial test of soil-rock mixture," *Computers & Geosciences*, vol. 73, pp. 179–188, 2016.

[25] Y. Wang, C. H. Li, and Y. Z. Hu, "Use of X-ray computed tomography to investigate the effect of rock blocks on meso-structural changes in soil-rock mixture under triaxial deformation," *Construction and Building Materials*, vol. 164, pp. 386–399, 2018.

[26] M. Afifipour and P. Moarefvand, "Mechanical behavior of bimrocks having high rock block proportion," *International Journal of Rock Mechanics and Mining Sciences*, vol. 65, pp. 40–48, 2014.

[27] Z. G. Gao and G. G. Liu, "Study on random aggregate model of two-dimensional concrete," *Journal of Tsinghua University (Science and Technology)*, vol. 43, no. 5, pp. 710–714, 2003.

[28] J. Zhang, N.-G. Jin, X.-Y. Jin, and J.-J. Zheng, "Numerical simulation method for polygonal aggregate distribution in concrete," *Zhejiang Daxue Xuebao (Gongxue Ban)/Journal of Zhejiang University (Engineering Science)*, vol. 38, no. 5, pp. 581–585, 2004.

[29] G. De Schutter and L. Taerwe, "Random particle model for concrete based on Delaunay triangulation," *Materials and Structures*, vol. 26, no. 2, pp. 67–73, 1993.

[30] Y. Zheng, C. Deng, S. Zhao, X. Tang, M. Liu, and L. Zhang, "Development of finite element limiting analysis method and its applications in geotechnical engineering," *International Journal of Engineering Science*, vol. 3, pp. 10–36, 2007.

[31] P. J. BARRETT, "The shape of rock particles, a critical review," *Sedimentology*, vol. 27, no. 3, pp. 291–303, 1980.

[32] L. Yan, Q. Meng, W. Xu et al., "A numerical method for analyzing the permeability of heterogeneous geomaterials based on digital image processing," *Journal of Zhejiang University-Science A*, vol. 18, no. 2, pp. 124–137, 2017.

[33] J. Kozicki, J. Tejchman, and Z. Mróz, "Effect of grain roughness on strength, volume changes, elastic and dissipated energies during quasi-static homogeneous triaxial compression using DEM," *Granular Matter*, vol. 14, no. 4, pp. 457–468, 2012.

[34] C. Wang and C.-N. Zhan, "Gravel content effect on the shear strength of clay-gravel mixtures," *Applied Mechanics and Materials*, vol. 71-78, pp. 4685–4688, 2011.

[35] Y. Li, R. Huang, L. S. Chan, and J. Chen, "Effects of particle shape on shear strength of clay-gravel mixture," *KSCE Journal of Civil Engineering*, vol. 17, no. 4, pp. 712–717, 2013.

[36] C. Nouguier-Lehon, B. Cambou, and E. Vincens, "Influence of particle shape and angularity on the behaviour of granular materials: A numerical analysis," *International Journal for Numerical and Analytical Methods in Geomechanics*, vol. 27, no. 14, pp. 1207–1226, 2003.

[37] X. Wen-Jie, X. Qiang, and H. Rui-Lin, "Study on the shear strength of soil-rock mixture by large scale direct shear test," *International Journal of Rock Mechanics and Mining Sciences*, vol. 48, no. 8, pp. 1235–1247, 2011.

[38] Y. Liu, J. Hu, H. Wei, and A.-L. Saw, "A direct simulation algorithm for a class of beta random fields in modelling material properties," *Computer Methods Applied Mechanics and Engineering*, vol. 326, pp. 642–655, 2017.